Bull. Mater. Sci., Vol. 37, No. 6, October 2014, pp. 1233–1241. © Indian Academy of Sciences.

Relaxor behaviour in $BaBi_4Ti_4O_{15}$ ceramics fabricated using the powders obtained by mechanochemically assisted synthesis route

SUNIL KUMAR and K B R VARMA*

Materials Research Centre, Indian Institute of Science, Bangalore 560 012, India

MS received 28 December 2013; revised 26 February 2014

Abstract. Mechanochemically activated reactants were found to facilitate the synthesis of fine powders comprising 200–400 nm range crystallites of $BaBi_4Ti_4O_{15}$ at a significantly lower temperature (700 °C) than that of solid-state reaction route. Reactants ($CaCO_3$, Bi_2O_3 and TiO_2) in stoichiometric ratio were ball milled for 48 h to obtain homogeneous mixture. The evolution of the $BaBi_4Ti_4O_{15}$ phase was systematically followed using X-ray powder diffraction (XRD) technique. Scanning electron microscopy (SEM) and transmission electron microscopy (TEM) were employed to probe its structural and microstructural details. The electron diffraction studies established the presence of correlated octahedral rotations and associated long-range polar ordering. High-resolution TEM imaging nevertheless revealed structural inhomogeneities leading to intergrowth defects. Dense $BaBi_4Ti_4O_{15}$ ceramics with an average grain size of 0·9 μm were fabricated using mechanochemically assisted synthesized powders at relatively low temperature (1000 °C). The effect of grain size on the dielectric and relaxor behaviour of $BaBi_4Ti_4O_{15}$ ceramics was investigated. Fine-grained ceramics (average grain size ~ 0·9 μm) showed higher diffusion in phase transition, lower temperature of phase transition, lower Vogel–Fulcher freezing temperature and higher activation energy for the polarization reversal than those for coarse-grained ceramics (average grain size ~ 7 μm) fabricated *via* the conventional solid-state reaction route.

Keywords. $BaBi_4Ti_4O_{15}$; mechanochemical synthesis; relaxor ferroelectrics; TEM; dielectric properties.

1. Introduction

Relaxors, that are characterized by the diffuse phase transition accompanied by the frequency dispersion of their phase transition temperatures, depict interesting physical properties which are relevant to advanced applications (Xu 1991; Cross 1994). Most literature that exists on relaxors constitutes the studies concerning the lead-based complex perovskites such as $Pb(Mg_{1/3}Nb_{2/3})O_3$, $(Pb_{1-x}La_{2x/3})(Zr_{1-y}Ti_y)O_3$, etc. (Bokov and Ye 2006). However, recently there has been a renewed interest on ferroelectrics that form viable alternates to lead-based ones as these suffer from inherent drawbacks. Among the lead-free relaxor ferroelectrics, those belonging to the Aurivillius family of oxides have drawn considerable attention mainly owing to their reltaively high Curie tempeartures (A-Paz De Araujo *et al* 1995; Park *et al* 1999). Aurivillius oxides have anisotropic layered structure associated with intergrowth of $[Bi_2O_2]^{2+}$ layers and $[A_{n+1}B_nO_{3n+1}]^{2-}$ pseudo-perovskite units, with n representing the number of perovskite-like layers stacked along the c-axis (Aurivillius 1950; Subarao 1962). $BaBi_4Ti_4O_{15}$ (BBT) is an $n = 4$ Aurivillius phase with Bi^{3+} and Ba^{2+} ions occupying the A-site in perovskite layers while Ti^{4+} ions occupying the B-site. BBT ceramics exhibit a relaxor-like diffused dielectric anomaly around 410 °C unlike other four-layered Aurivillius phases that include $SrBi_4Ti_4O_{15}$ and $CaBi_4Ti_4O_{15}$ (Tellier *et al* 2004; Rout *et al* 2009; Bobić *et al* 2010).

Recently, many groups have reported the details pertaining to the fabrication and electrical properties of doped and undoped BBT ceramics. In most reports, BBT starting powders were synthesized *via* the solid-state reaction route by mixing the constituent oxides followed by different calcination steps at high temperatures (950 + 1050 °C) with intermittent grindings (Pribošič *et al* 2001; Hou *et al* 2006; Kumar and Varma 2009, 2010, 2011). However, there exists few reports on the preparation of BBT powders using non-conventional methods such as the Pechini method (Murugan *et al* 2006), sol–gel (Xie and Pan 2003; Rout *et al* 2009), templated grain growth (Kimura and Yoshida 2006), and molten-salt synthesis (Huang *et al* 2011). Calcination of reactant oxides at high temperatures generally results in the coarsening and agglomeration of particles and compositional fluctuations in materials synthesized using solid-state reaction route. Further, it may result in non-stoichiometry due to the volatilization of oxides (particularly Bi-based) during high temperature calcination and sintering. Synthesis associated with mechanochemical route would help to

*Author for correspondence (kbrvarma@mrc.iisc.ernet.in)

overcome these problems to a certain extent. A wide range of ferroelectric materials, including those belonging to Aurivillius oxides, has been made using mechanical activation and extensively investigated for their physical properties (Lisoni *et al* 2001; Sim *et al* 2004; Ferrer *et al* 2007; Lazarević *et al* 2009a,b). Lazarević *et al* (2009a) have reported the formation of BBT by heating the homogenized mixture of $BaTiO_3$ and $Bi_4Ti_3O_{12}$ at 1100 °C for 4 h (Lazarević *et al* 2009a,b). The focus of the present work was to study the feasibility of forming nanocrystalline BBT powders using mechanochemical route and to note whether these could be sintered at relatively low temperatures than that of solid-state reaction route. Transmission electron microscopy (TEM) and the dielectric and ferroelectric properties of the ceramics fabricated using fine powders obtained by mechanochemically assisted synthesis are reported in the following sections.

2. Experimental

Mechanical activation technique has been used to synthesize BBT powders. For this, 10 g of Bi_2O_3, Ba_2CO_3 and TiO_2 in stoichiometric ratio were mixed thoroughly using an agate mortar. Then the mixture was placed in agate vessel containing 11 agate balls each having a diameter of 5 mm and was mechanically activated in a planetary mill (Fristch, Pulverisette model P7). The milling bowl of the planetary system was rotated at 350 rpm. Milling was carried out in propanol medium and was stopped for 10 min after every 30 min to cool down the system. The mixed slurry was dried at 150 °C for complete removal of propanol. XRD patterns at room temperature for milled powders and that heated at various temperatures were obatined using Bruker-D8 Advance diffractometer with CuKα radiation in the 2θ range of 10–60° at a step width of 0·019°. The powder was ground again and mixed with a small amount of polyvinyl alcohol (PVA) as a binder. Resultant powders were then pressed uniaxially under a pressure of 200 MPa into cylindrical pellets of diameter 10–12 and 1–2 mm in thickness. The binder was burnt out by slowly heating the pellets at 500 °C for 2 h. These were sintered at 900–1050 °C for 3 h in air at a heating rate of 3 °C/min and then furnace was cooled to room temperature. Densities of the sintered pellets were measured by the Archimedes method using xylene (room temperature density ~ 0·86 g/cm^3) as the liquid medium. For comparative studies, BBT ceramics were also fabricated *via* the conventional solid-state reaction route by calcining the stoichiometric mixture of Bi_2O_3, Ba_2CO_3 and TiO_2 at 950 °C for 10 h and 1050 °C for 10 h with intermittent grinding and subsequent sintering at 1100–1200 °C for 3 h.

Scanning electron microscope (SEM) equipped with energy dispersive X-ray spectrometry (EDX) (Quanta-ESEM, FEI) was used for microstructural and compositional analyses. TEM study was carried out using a Tecnai-T20 TEM (FEI, operated at 200 kV) equipped with a double-tilt rotating sample holder. Specimens for TEM were prepared by sonicating the dispersed polycrystalline BBT powder in acetone medium and putting a drop of this dispersion on a copper grid-supported carbon thin film. The fast Fourier transform (FFT) patterns were obtained by using the Gatan Digital Micrograph software (Gatan Inc.).

For electrical property measurements, silver electrodes were deposited on either side of polished surfaces of the pellet and was baked at 200 °C for 2 h to dry out the moisture prior to any measurement. Capacitance and dielectric loss were measured using an impedance analyser (Model 4192A, Hewlett-Packard) at signal strength of 0·5 V in the 27–450 °C temperature range at various frequencies (10 kHz to 1 MHz). The ferroelectric polarization–electric field (*P–E*) loop (50 Hz) was obtained by a ferroelectric hysteresis loop tracer (Marine India Inc.) at room temperature.

3. Results and discussion

3.1 *X-ray diffraction*

Figure 1 shows the XRD patterns of a mixture of $BaCO_3 : 2Bi_2O_3 : 4TiO_2$ ball milled for 48 h together with those heated at different temperatures. The formation of amorphous phase on subjecting the $2Bi_2O_3 : 3TiO_2$ mixture

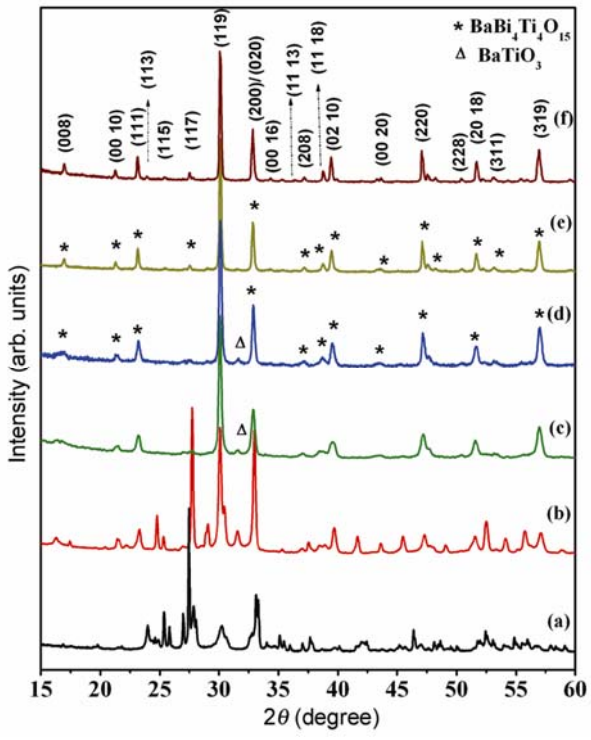

Figure 1. XRD patterns for (a) $BaCO_3 : 2Bi_2O_3 : 4TiO_2$ mixture ball-milled for 48 h and milled powders heated at (b) 400 °C, (c) 500 °C, (d) 600 °C, (e) 700 °C and (f) 800 °C for 5 h.

to 12 h of planetary ball milling was reported in the literature (Lisoni *et al* 2001; Ferrer *et al* 2007). In the present study, we could not obtain the amorphous phase even after 48 h of ball milling. However, the XRD pattern for the milled mixture (figure 1a) shows significantly broad and low intensity peaks. Most of these peaks could be indexed to the reactant oxides. To facilitate the formation of BBT phase, mechanically activated precursors were heated at various temperatures. Figure 1(b)–(f) shows the XRD patterns recorded for the powders heated at 400, 500, 600, 700 and 800 °C for 5 h, respectively. XRD pattern for the powder heated at 400 °C (figure 1b) indicates the formation of a mixed phase with peaks corresponding to reactant oxides and intermediate phases (possibly $BaTiO_3$, $Bi_2Ti_2O_7$ and $Bi_2Ti_4O_{11}$). XRD pattern recorded for the powder heated at 500 °C (figure 1c) shows broad peaks corresponding to BBT along with the presence of an impurity peak at 31·6°. On further increasing the heat treatment temperature, intensities of the peaks corresponding to BBT phase increased while the peak at 31·6° diminished and disappeared for the powder heated at 700 °C/5 h (figure 1e). The only phase remaining at 700 °C and above is BBT. Further increase in heat treatment temperature resulted in an increase in the intensities of BBT peaks suggesting an increase in the crystallite size.

3.2 *Microstructural analysis*

Figure 2(a) and (b) shows the scanning electron micrographs of the stoichiometric mixture of oxides/carbonate obtained after milling for 48 h in the planetary mill. The milled powder consisted of fine particles in the 60–90 nm range associated with spherical morphology. Of course, one would also notice the presence of agglomerates in the same picture. Scanning electron micrographs of activated mixture of reactants heated at 400 and 500 °C for 5 h are shown in figure 2(c) and (d). Changes in the morphology accompanied by an increase in the particle size of milled powder have been found during the formation of BBT phase. As evidenced by the XRD pattern of the powder heated at 500 °C (figure 1c), it is a mixture of BBT phase and the secondary phase ($BaTiO_3$) which explains the existence of different morphologies and dispersion in crystallite size. The effect of heat treatment on the morphology and crystallite size is more pronounced in the samples heated at 600 °C and above as shown in figure 3(a)–(d). The morphology of the crystallites is strikingly different from those of as-milled powders. Crystallites in these samples are platelet-like which is a characteristic feature of layered Aurivillius oxides and is attributed to their anisotropic crystal structure. With the increase in temperature of heat treatment, the crystallite size as expected increased associated with a pronounced crystal habit. This is in agreement with the increase in crystallinity observed by XRD.

In order to probe further into the influence of mechanochemical activation on the sintering behaviour, uniaxially pressed green pellets of BBT were sintered at different temperatures. The scanning electron micrographs for the pellets sintered at 900, 950 and 1000 °C for 3 h are

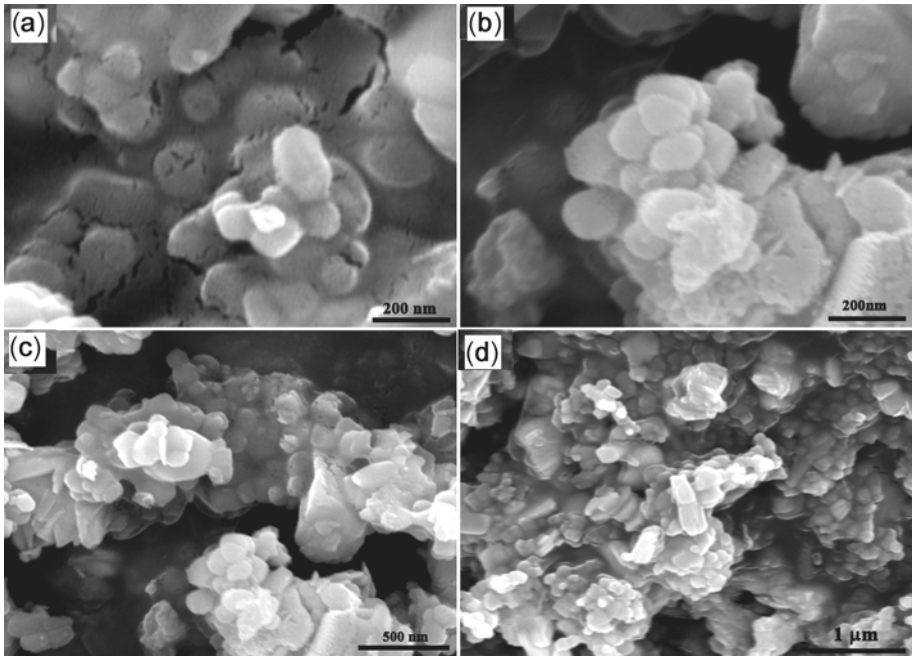

Figure 2. Scanning electron micrographs of mixture of initial reactants ($BaCO_3$, Bi_2O_3 and TiO_2) subjected to 48 h of ball-milling (**a**) and (**b**), activated mixture of reactants heated at 400 °C for 5 h (**c**) and at 500 °C for 5 h (**d**).

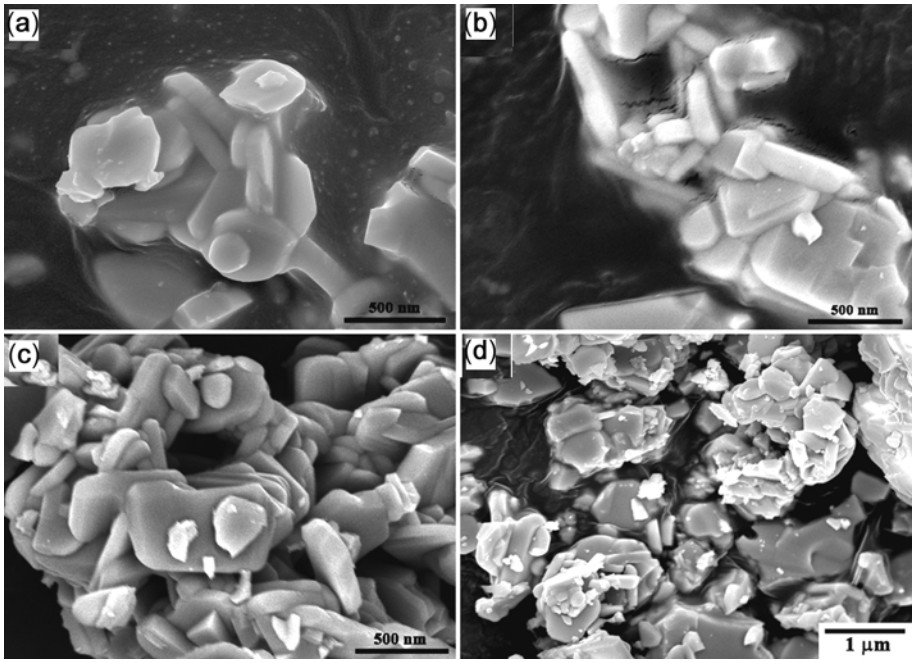

Figure 3. SEM images of activated mixture of reactants heated at (**a**) 600 °C for 5 h, (**b**) 700 °C for 5 h, (**c**) 800 °C for 5 h and (**d**) 900 °C for 5 h.

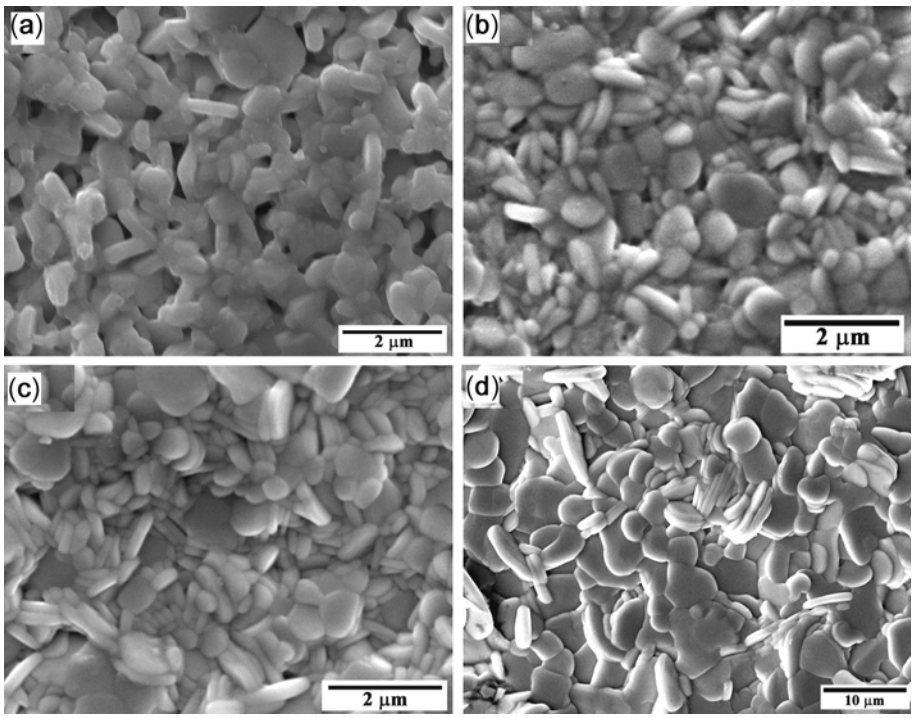

Figure 4. SEM images of $BaBi_4Ti_4O_{15}$ pellets (BBT-MCA) sintered at (**a**) 900 °C, (**b**) 950 °C, (**c**) 1000° C for 3 h and (**d**) ceramics fabricated *via* the conventional solid-state reaction route and sintered at 1150 °C for 3 h (BBT-SS).

shown in figure 4(a–c). Pellet sintered at 900 °C for 3 h (figure 4a) has an average grain size of ~0·6 μm with larger intergranular pores resulting in poor density (relative density ~81%). Increase in the sintering duration slightly improved the relative density (up to 85% for pellet sintered for 12 h). As expected, increase in the sintering temperature resulted in an increase in the average grain size and density. Pellets sintered at 950 and 1000 °C for

3 h (figure 4(b) and (c), respectively) revealed well-packed, randomly oriented plate-like grains typical of Aurivillius family of oxides. The relative densities for these pellets were around 93% and 95%. Further increase in the sintering temperature resulted in an anomalous grain growth (not shown here) accompanied by poor density. Anomalous grain growth with increased aspect ratio hinders the densification process (Sim *et al* 2004). The optimum sintering temperature to achieve the maximum density for the BBT ceramics processed *via* the conventional solid-state reaction route was found to be 1150 °C. Relative density of the ceramics sintered at this temperature for 3 h was found to be ~ 95% of the theoretical density. Scanning electron micrograph (figure 4d) for these ceramics shows the relatively large grains with an average size around 7 μm. High reactivity and smaller particle size of the BBT powder obtained *via* mechanochemical-assisted synthesis facilitate the sintering process which allows one to obtain high density ceramics at relatively lower temperatures than those fabricated using BBT powders synthesized using the conventional solid-state reaction route.

3.3 *Transmission electron microscopy*

Representative bright field TEM image of the thin crystallite of BBT powder with [0 0 1] orientation parallel to the electron beam is shown in figure 5(a). The corresponding SAED pattern in figure 5(b) shows a near four-fold symmetry as the lattice parameters a and b are almost equal. The most intense spots in the electron diffraction pattern could be indexed to the room temperature orthorhombic cell with a and b parameters equal to ~ 0·545 nm. In addition to the bright fundamental reflections, weak superlattice reflections at the 1/2{h, k, 0}, 1/2 {h, 0, 0} and 1/2 {0, k, 0} positions are present in the SAED pattern (figure 5b). 1/2 {h, k, 0} (with $h \neq k$) type of reflections are attributed to the inphase octahedral rotations and the associated cation displacements, leading to 1/2 {h, 0, 0}, 1/2 (0, k, 0} type of reflections (Glazer 1972; Reaney *et al* 1994; Suárez *et al* 2001). The forbidden reflections like 1/2 {h k 0} with $h = k$ also appear in [0 0 1] zone *via* double diffraction route, for instance 1/2 {–2 0 0} + 1/2 {3 1 0} = 1/2 {1 1 0}. The superlattice reflections occur at half-integral positions because of the cell doubling caused by octahedral rotations. The presence of superlattice reflections in the SAED pattern confirms the collective octahedral rotations and associated distortion in BBT. A high-resolution TEM (HRTEM) image of crystal oriented along the [0 0 1] zone-axis is shown in figure S1 (see supplementary information). Fringes with lattice spacing ~ 0·38 nm that correspond to the lattice parameter a of the prototype tetragonal unit cell are marked. Figure 6 shows a HRTEM image of the BBT crystal recorded along the [1 0 0]/[0 1 0] zone-axis. Corresponding fast FFT is shown in the inset. The modulated structures of the perovskite layers and bismuth oxide layers along the c-axis in BBT are readily observed. The observed image contrast suggests that the periodic fringes with a spacing of ~ 2·09 nm (averaged over a large area) correspond to Bi_2O_2 layers. The lattice parameter of the c-axis is measured to be 4·18 nm, which is in good agreement with the structural data obtained from the refinement of XRD data. On closer inspection, one would see that thickness of the perovskite slabs (sandwiched between the Bi_2O_2 layers) is not uniform. The magnified regions of the HRTEM image that is depicted in figure 6 are shown in figure S2 (a and b). The lattice parameter c of an n-layered Aurivillius phase is

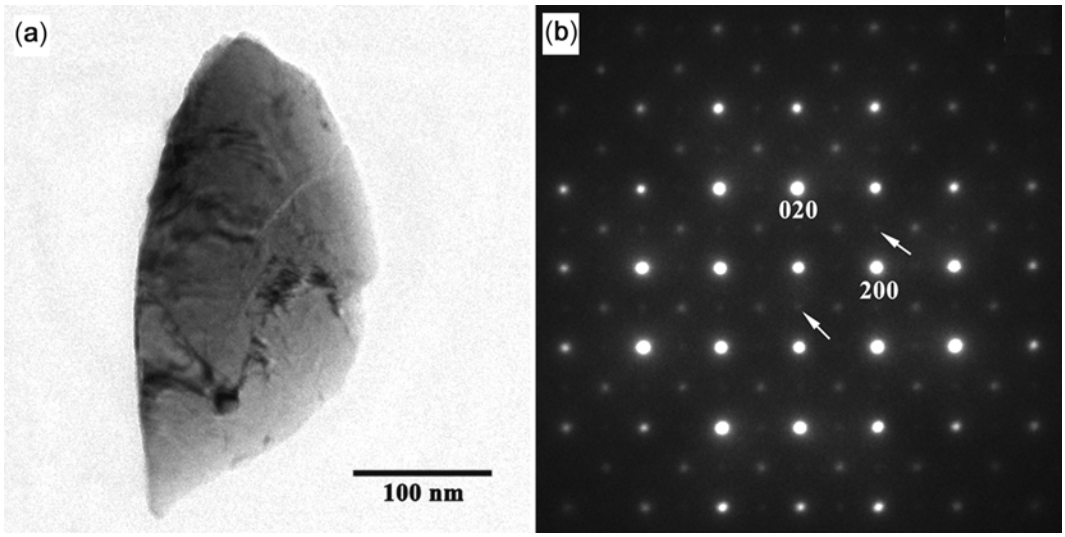

Figure 5. (**a**) Bright field TEM image and (**b**) [0 0 1] selected-area diffraction pattern of the BBT crystal. The superposition of the orthogonal diffraction patterns from the two 90° domain variants lead to an apparent four-fold symmetry. Superlattice spots are indicated by arrows.

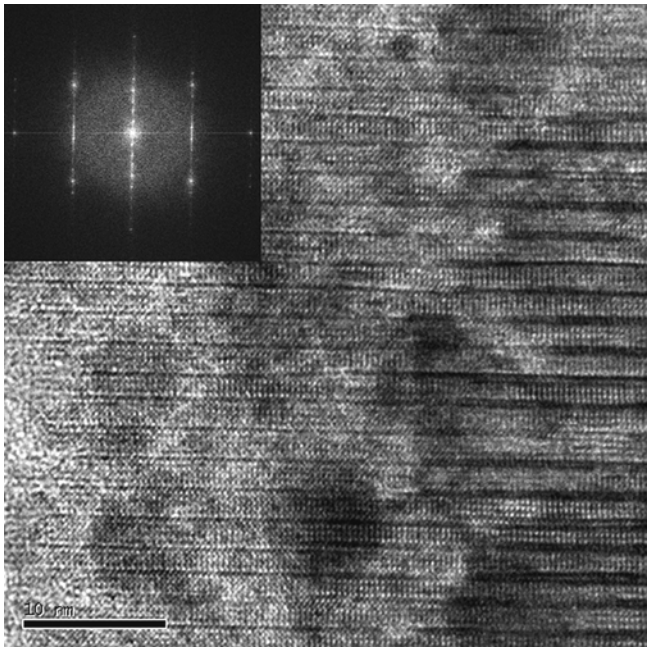

Figure 6. High-resolution electron micrograph of a crystal of $BaBi_4Ti_4O_{15}$ recorded along the [1 0 0] direction. Insets show the corresponding FFTs.

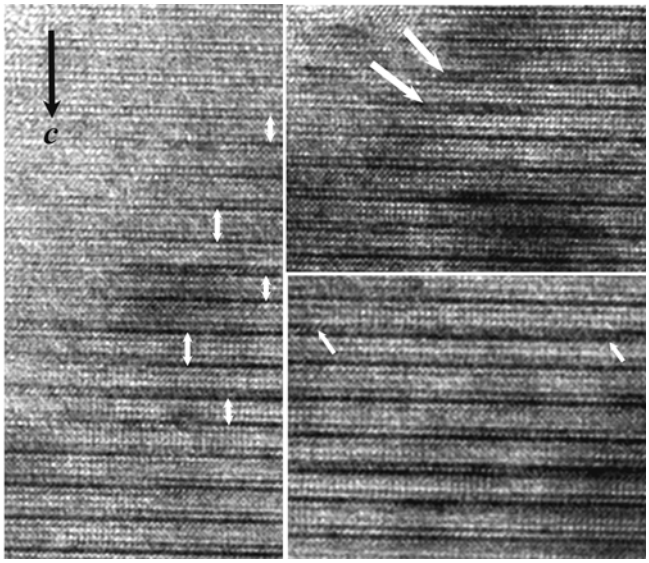

Figure 7. High-resolution electron micrograph of a crystal of $BaBi_4Ti_4O_{15}$ recorded along the [1 1 0] direction. Double headed arrows suggest non-uniform thickness of perovskite slabs.

approximately $2nC_p + 2C_B$, where $C_p \sim 0{\cdot}4$ nm and $C_B \sim 0{\cdot}45$ nm are the thickness of ABO_3-type block and Bi_2O_2 layer, respectively. Accordingly, c for an $n = 4$ Aurivillius phase is expected to be around 4·1 nm which is indeed confirmed by the XRD studies for BBT. As seen in figure 6, bands of thickness around 1·2 nm (corresponds to three-ABO_3 blocks) and 2 nm (corresponds to five-ABO_3 blocks) are also present in BBT. However, there is no regular intergrowth of bands and these defects are randomly distributed unlike higher order Aurivillius phases where regular intergrowths of lower order members are often seen (Kikuchi 1976; Hutchison *et al* 1977; Gopalakrishnan *et al* 1984; Boullay and Mercurio 2004).

HRTEM images of another BBT crystal recorded along the [1 1 0] zone axis is shown in figure 7. In addition to stacking faults, HRTEM carried out on different crystals of BBT showed the presence of shearing defects. These defects keep the global stoichiometry unchanged with the same thickness of perovskite slabs. In figure 7, the cationic row belonging to the Bi_2O_2 layer in the average structure contains some non-Bi cations from the adjacent octahedron. Structural refinements for BBT have indeed confirmed that the fluorite (Bi_2O_2) layers contain a significant amount of Ba^{2+} ions (Tellier *et al* 2004). Similar inclusion of an extra perovskite slab, along with the progressive sidestepping of Bi_2O_2 layers, was also observed in $Ba_2Bi_4Ti_5O_{18}$ (Hutchison and Smith 1981). Interestingly, both $BaBi_4Ti_4O_{15}$ and $Ba_2Bi_4Ti_5O_{18}$ show relaxor behaviour. Such correlation between the intergrowth defects and phase transition behaviour in other ferroelectrics belonging to Aurivillius family of oxides need to be further probed. It is to be noted that FFT shown in the inset of figure 6 confirms a strong streaking along the c-axis. This is associated with the high concentrations of randomly distributed intergrowth defects.

3.4 *Dielectric and ferroelectric properties*

The temperature dependence of the dielectric constant (ε_r) and loss tangent (D) of BBT ceramics fabricated using fine powders obtained by mechanochemically assisted synthesis and sintered at 1000 °C for 3 h (henceforth called as BBT-MCA) at three different frequencies (10, 100 and 1000 kHz) are depicted in figure 8(a). Dielectric constant exhibits a broad peak around 400 °C and the temperature of the dielectric maximum (T_m) shifts towards higher temperature from 396 to 410 °C with the increase in frequency from 10 to 1000 kHz. Temperature range in which this dielectric anomaly occurs coincides with the change in the crystal structure of BBT from orthorhombic (space group $A2_1am$) to tetragonal (space group $I4/mmm$), suggesting it to be a ferroelectric to paraelectric phase transition. This type of relaxation behaviour is in consistence with the other reports and confirms the relaxor nature of the present ceramics (Hou *et al* 2006; Kumar and Varma 2009; Rout *et al* 2009; Bobić *et al* 2010; Kumar and Varma 2010). The dielectric loss also exhibits a similar anomaly in the 400–410 °C temperature range. The values for the room temperature (27 °C) dielectric constant and loss at 100 kHz are 166 and 0·032, respectively. Dielectric constant (ε_r)

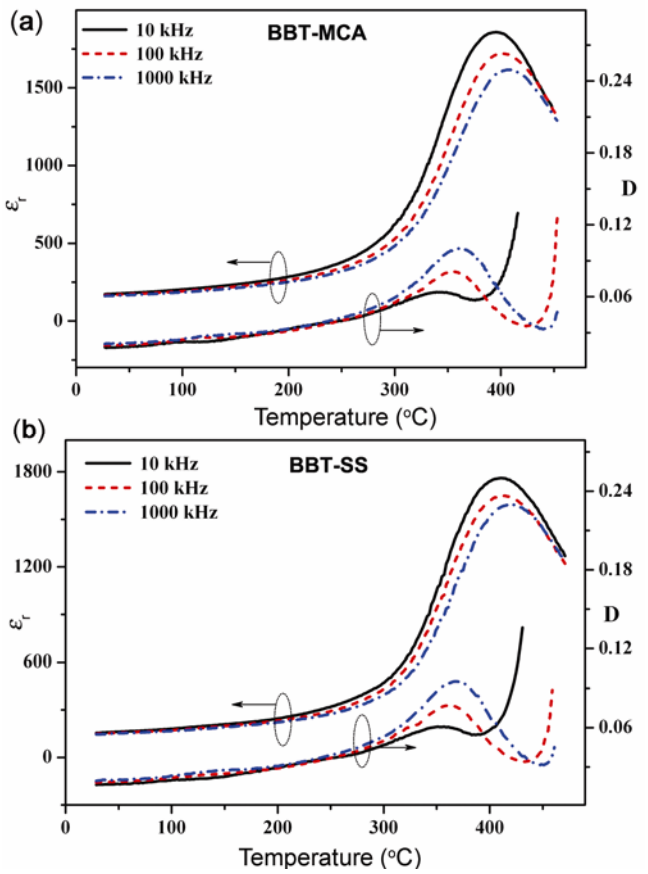

Figure 8. Temperature dependence of the dielectric constant (ε_r) and dielectric loss (D) measured at 10, 100 and 1000 kHz for the $BaBi_4Ti_4O_{15}$ ceramics: (**a**) BBT-MCA and (**b**) BBT-SS.

and loss tangent (D) of BBT ceramics fabricated *via* the conventional solid-state reaction route and sintered at 1150 °C for 3 h (henceforth called as BBT-SS) as a function of temperature at three different frequencies are shown in figure 8(b). BBT-SS ceramics exhibit typical relaxor behaviour with a frequency-dependent temperature of dielectric maximum. Summary of the properties of BBT-MCA and BBT-SS ceramics is illustrated in table 1. As compared to the ceramics fabricated by solid-state reaction route (BBT-SS) with larger average grain size (7 μm), value for room temperature dielectric constant is higher for the BBT-MCA ceramics whereas T_m is lower (402 °C as opposed to 415 °C for BBT-SS). It is known that internal stresses developed in ceramics during the cooling, through the Curie temperature, are higher in fine grained ceramics than in coarse-grained ceramics, as the smaller grain size constraints the formation of stress-relieving non-180° domains. Resulting internal stresses in fine-grained ceramics tend to reduce the Curie temperature and enhance the dielectric constant (Randall *et al* 1998; Deng *et al* 2006; Jiménez *et al* 2008; Zhang *et al* 2009) which is consistent with the results obtained in the present investigation. Increase in the value of dielectric loss for BBT-MCA ceramics is attributed to the increased domain density (Randall *et al* 1998).

Table 1. Room temperature dielectric constant (ε_r), dielectric loss (D), degree of diffuseness (γ), temperature of phase transition (T_m) measured at 100 kHz, remnant polarization (P_r) and coercive field (E_C) for BBT ceramics.

Sample	BBT-MCA	BBT-SS
Grain size (μm)	0·9	7
ε_r	166	148
D	0·019	0·017
T_m (°C)	402 ± 2	415 ± 2
γ	1·816 ± 0·008	1·76 ± 0·02
P_r (μC/cm^2)	4·3	5·4
E_C (kV/cm)	40·4	38·2

Generally, the empirical relation which is a modified form of Curie–Weiss law, proposed by Uchino and Nomura (1982) is used to describe the variation of dielectric constant as a function of temperature above T_m for relaxors. The relation is given by

$$\frac{1}{\varepsilon_r} = \frac{1}{\varepsilon_m} + \frac{(T - T_m)^\gamma}{C}, \tag{1}$$

where ε_m is the maximum value of the dielectric constant at the transition temperature (T_m), C the Curie-like constant and γ the degree of diffuseness. The limiting values 1 and 2 for γ, respectively, reduce the expression to the Curie–Weiss law valid for a normal and the quadratic dependence for the complete diffuse phase transition. Insets in figure 9(a) and (b) show the plots of $\ln(1/\varepsilon_r - 1/\varepsilon_m)$ vs $\ln(T - T_m)$ at 100 kHz for BBT-MCA and BBT-SS ceramics. By fitting the experimental data in (1), the values obtained for γ are 1·816 ± 0·008 and 1·76 ± 0·02 for BBT-MCA and BBT-SS ceramics, respectively. Higher value obtained for γ for fine-grained (BBT-MCA) ceramics implies an increase in the diffusive nature of the phase transition and is ascribed to the grain size effects. Relaxor ferroelectrics are known to follow an empirical Vogel–Fulcher (VF) relationship (Cross 1994)

$$f = f_o \exp\left[\frac{-E_a}{k_B(T_m - T_{VF})}\right], \tag{2}$$

where E_a and T_{VF} are the activation energy and the static freezing temperature, k_B the Boltzmann constant and f_o the pre-exponential factor. Variation of T_m with $\ln(f)$ for both the samples is shown in figure 9. Temperature of dielectric peak T_m shows good fits to the Vogel–Fulcher relation, corroborating the existence of relaxor behaviour in both BBT-MCA and BBT-SS ceramics. From the non-linear VF fitting (figure 9a and b), values of the fitting parameters f_o, E_a and T_{VF} were found to be $1{\cdot}3 \times 10^9$ Hz, 0·025 ± 0·004 eV and 372 ± 2 °C, respectively, for the

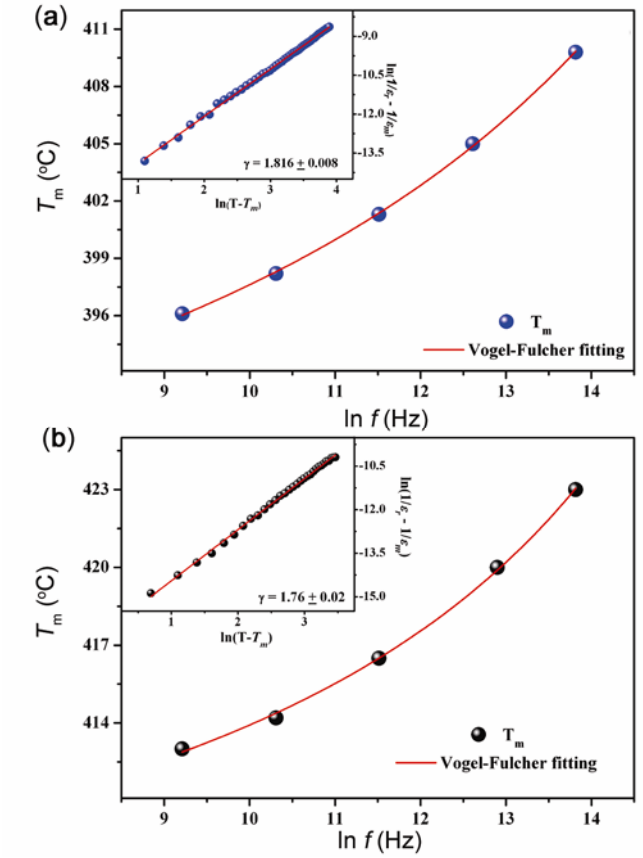

Figure 9. Temperature of dielectric maximum (T_m) as a function of ln(f) for (**a**) BBT-MCA and (**b**) BBT-SS ceramics. The *symbols* represent the experimental data and the *solid line* is the fitting to (1). Insets of figure 13(a) and (b) show the plots of log $(1/\varepsilon_r - 1/\varepsilon_m)$ vs log$(T - T_m)$ for BBT-MCA and BBT-SS ceramics, respectively.

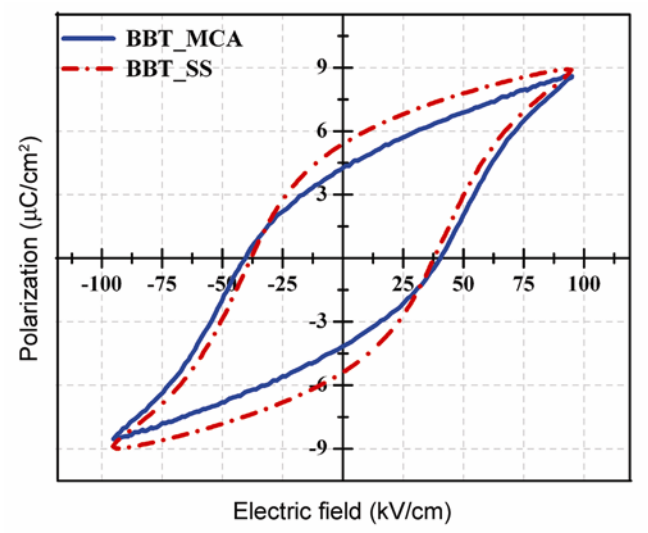

Figure 10. Ferroelectric hysteresis loops for $BaBi_4Ti_4O_{15}$ ceramics of two different grain sizes recorded at room temperature under an applied maximum electric field of 95 kV/cm at 50 Hz.

fine-grained BBT-MCA ceramics and $1{\cdot}7 \times 10^8$ Hz, $0{\cdot}011 \pm 0{\cdot}003$ eV and coarse-grained BBT-SS ceramics 400 ± 2 °C. It is widely believed that the dielectric properties of relaxor ferroelectrics are governed by the dynamics of the polar nanoregions (PNRs). Higher concentration of grain boundaries and associated internal stresses in fine grained ceramics could affect the dynamics of these PNRs. Studies on size effects in $(PbMg_{1/3}Nb_{2/3}O_3)_{0{\cdot}65}$–$(PbTiO_3)_{0{\cdot}35}$ have shown the appearance of relaxor behaviour in ceramics with grain size below 200 nm associated with convolution of macroscopic ferroelectric domains towards locally ordered PNRs embodied in paraelectric matrix (Carreaud *et al* 2005). Reduction in grain size is indeed known to enhance/induce the relaxor behaviour as a consequence of domain refinement and weakening of the long-range polar ordering in fine-grained ceramics (Tan and Viehland 1997; Randall *et al* 1998; Carreaud *et al* 2005; Tang and Chan 2005; Jiménez *et al* 2008; Zhang *et al* 2009).

Ferroelectric nature of BBT ceramics obtained *via* the mechano-activation process was confirmed by the demonstration of polarization (P) vs electric field (E) hysteresis loop. P–E loops recorded for BBT-MCA and BBT-SS ceramics at room temperature are shown in figure 10. A remnant polarization (P_r) of $4{\cdot}3$ μC/cm^2 and a coercive field (E_c) of $40{\cdot}4$ kV/cm under an applied electric field of 95 kV/cm are obtained for the BBT-MCA ceramics. These studies revealed that both saturation polarization and remnant polarization obtained for the fine-grained BBT-MCA ceramics are lower than that of BBT-SS ceramics whereas the coercive field is slightly higher. The rectangular ratio of the hysteresis loops, defined as P_r/P_{max} where P_r is the remnant polarization and P_{max} is the maximum polarization, is lower for BBT-MCA ceramics which suggests that the ferroelectric switching is much more difficult in fine-grained sample. As the ferroelectric switching process is a transgranular cooperative phenomenon, reduction in grain size usually affects the domain size, domain density, domain wall mobility and domain walls–grain boundary coupling (Randall *et al* 1998). Increased concentration of grain boundaries in fine-grained samples increases the strong coupling between the domain walls and grain boundaries thereby making the domain reorientation more difficult and inhibiting the domain wall motion (Tan and Viehland 1997; Randall *et al* 1998; Tang and Chan 2005). The reduction of the achievable domain alignment manifests itself in the lower value of remnant polarization.

4. Conclusions

In summary, monophasic BBT powder was synthesized by heating the mechanically activated precursors at 700 °C for 5 h. Detailed structural studies were carried

out using XRD and TEM. Mechano-activation facilitated a reduction in the sintering temperature for BBT with a relative density ~ 95% of theoretical density (achievable in ceramics sintered at 1000 °C for 3 h). Superlattice reflections were observed in SAED pattern recorded along the [0 0 1] zone-axis confirming a tilt in the octahedra. HRTEM images showed the stacking faults in perovskite blocks along the *c*-axis. Dielectric characterization showed a frequency-dependent diffuse phase transition around 400 °C which follows the Vogel–Fulcher relation, confirming the relaxor nature. BBT ceramics sintered at 1000 °C for 3 h exhibited a room temperature dielectric constant of 166 and loss tangent of 0·019 (both at 100 kHz). Dielectric and ferroelectric properties of thus prepared fine-grained ceramics were compared with coarse-grained (grain size ~ 7 μm) ceramics fabricated via the conventional solid-state reaction route. Fine-grained ceramics (average grain size ~ 0·9 μm) showed a higher diffuseness in phase transition, lower temperature of phase transition, lower Vogel–Fulcher freezing temperature and higher activation energy for the polarization reversal than those for coarse-grained ceramics.

Electronic Supplementary Material

Supplementary material pertaining to this article is available on the Bulletin of Materials Science website (www.ias.ac.in/matersci).

References

A-Paz De Araujo C, Cuchlaro J D, McMillan L D, Scott M C and Scott J F 1995 *Nature* **374** 627

Aurivillius B 1950 *Ark. Kemi* **2** 519

Bobić J D, Vijatović M M, Greičius S, Banys J and Stojanović B D 2010 *J. Alloys Compd.* **499** 221

Bokov A A and Ye Z G 2006 *J. Mater. Sci.* **41** 31

Boullay P and Mercurio D 2004 *Intergr. Ferroelectcr.* **62** 149

Carreaud J, Gemeiner P, Kiat J M, Dkhil B, Bogicevic C, Rojac T and Malic B 2005 *Phys. Rev.* **B72** 174115

Cross L E 1994 *Ferroelectrics* **151** 305

Deng X, Wang X, Wen H, Chen L and Li L 2006 *Appl. Phys. Lett.* **88** 252905

Ferrer P, Algueró M, Iglesias J E and Castro A 2007 *J. Eur. Ceram. Soc.* **27** 3641

Glazer A M 1972 *Acta Crystallogr.* **B28** 3384

Gopalakrishnan J, Ramanan A, Rao C N R, Jefferson D A and Smith D J 1984 *J. Solid State Chem.* **55** 101

Hou R Z, Chen X M and Zeng Y W 2006 *J. Am. Ceram. Soc.* **89** 2839

Huang J, Li L, Gu Y and Li Q 2011 *Adv. Mater. Res.* **335–336** 704

Hutchison J L, Anderson J S and Rao C N R 1977 *Proc. R. Soc. London Ser.* **A355** 301

Hutchison J L and Smith D J 1981 *Acta Crystallogr.* **A37** 119

Jiménez R, Amorín H, Ricote J, Carreaud J, Kiat J M, Dkhil B, Holc J, Kosec M and Algueró M 2008 *Phys. Rev.* **B78** 094103

Kikuchi T 1976 *J. Less-Common Met.* **48** 319

Kimura T and Yoshida Y 2006 *J. Am. Ceram. Soc.* **89** 869

Kumar S and Varma K B R 2009 *J. Phys. D: Appl. Phys.* **42** 075405

Kumar S and Varma K B R 2010 *Adv. Sci. Lett.* **3** 20

Kumar S and Varma K B R 2011 *Curr. Appl. Phys.* **11** 203

Lazarević Z Ž, Bobić J, Romčević N Ž, Paunović N and Stojanović B D 2009a *Sci. Sinter.* **41** 329

Lazarević Z Z, Romčević N Z, Bobić J D, Romčević M J, Dohčević-Mitrović Z and Stojanović B D 2009b *J. Alloys Compd.* **486** 848

Lisoni J G, Millán P, Vila E, Martín de Vidales J L, Hoffmann T and Castro A 2001 *Chem. Mater.* **13** 2084

Murugan A V, Navale S C and Ravi V 2006 *Mater. Lett.* **60** 1023

Park B H, Kang B S, Bu S D, Noh T W, Lee J and Jo W 1999 *Nature* **401** 682

Pribošič I, Makovec D and Drofenik M 2001 *J. Eur. Ceram. Soc.* **21** 1327

Randall C A, Kim N, Kucera J P, Cao W and Shrout T R 1998 *J. Am. Ceram. Soc.* **81** 677

Reaney I M, Colla E L and Setter N 1994 *Jpn. J. Appl. Phys., Part 1* **33** 3984

Rout S K, Sinha E, Hussian A, Lee J S, Ahn C W, Kim I W and Woo S I 2009 *J. Appl. Phys.* **105** 024105

Sim M H, Xue J M and Wang J 2004 *Mater. Lett.* **58** 2032

Suárez D Y, Reaney I M and Lee W E 2001 *J. Mater. Res.* **16** 3139

Subarao E C 1962 *J. Am. Ceram. Soc.* **45** 166

Tan Q and Viehland D 1997 *Ferroelectrics* **193** 157

Tang X G and Chan H L W 2005 *J. Appl. Phys.* **97** 034109

Tellier J, Boullay P, Manier M and Mercurio D 2004 *J. Solid State Chem.* **177** 1829

Uchino K and Nomura S 1982 *Ferroelectrics* **44** 55

Xie D and Pan W 2003 *Mater. Lett.* **57** 2970

Xu Y 1991 *Ferroelectric materials and their applications* (Amsterdam: Elsevier)

Zhang H, Yan H, Ning H, Reece M J, Eriksson M, Shen Z, Kan Y and Wang P 2009 *Nanotechnology* **20** 385708